
Flux balance network expansion predicts stage-specific human peri-implantation embryo metabolism

Andisheh Dadashi^{1,2*}, Derek Martinez³,

1 Division of Mathematics, Engineering, and Computer Science, The University of New Mexico-Valencia, Los Lunas, NM, USA 87031

2 Department of Computer Science, University of New Mexico, Albuquerque, NM, USA

3 The Science and Wellness Division, The University of New Mexico-Valencia, Los Lunas, NM, USA 87031

* andisheh@unm.edu

Appendix A. Supporting information

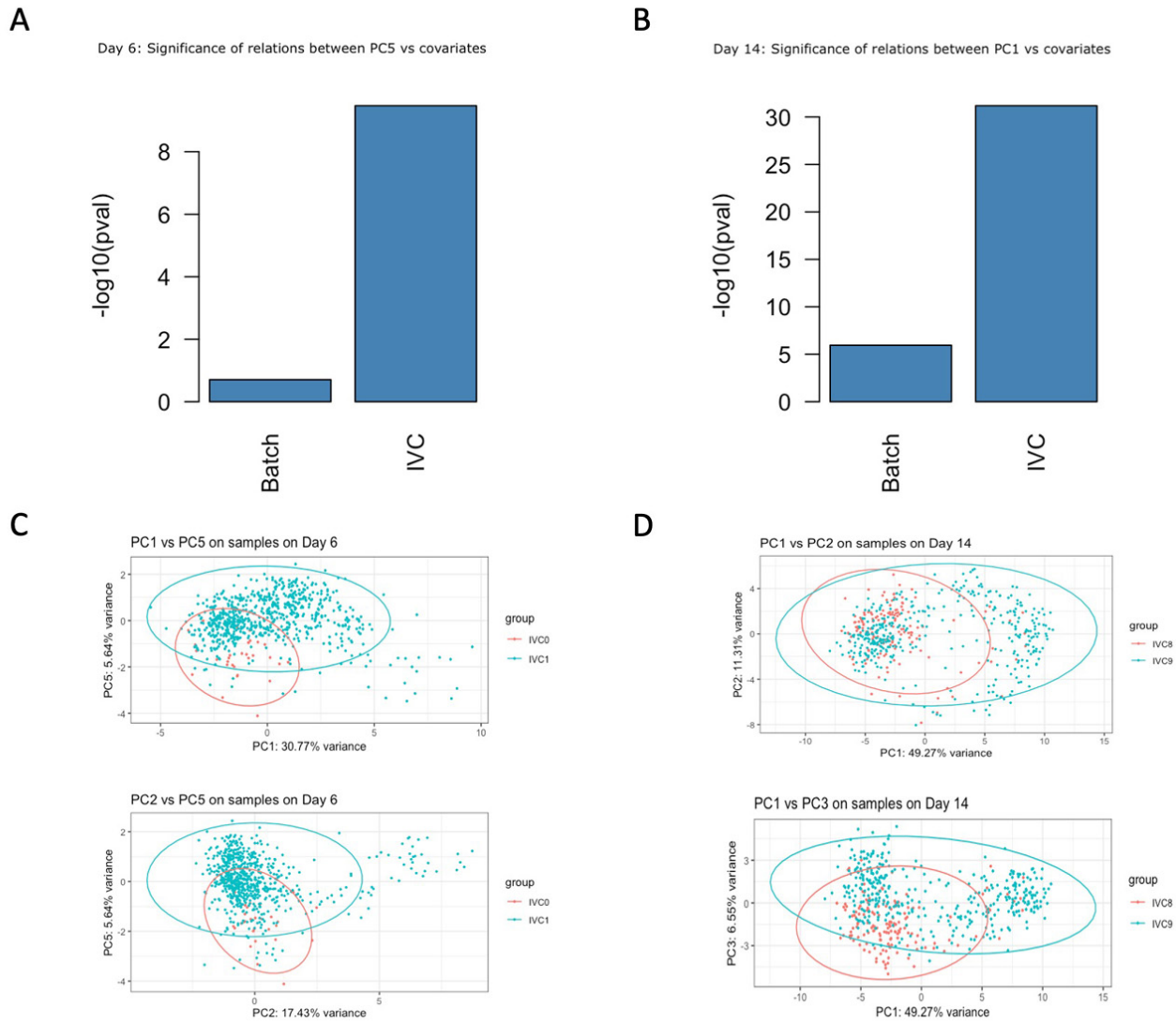


Fig.A 1: Principal component analysis. (A-B) Significant covariates are shown for stage 1 (day 6), and stage 5 (day 14). Relation of two main variables IVC and batch effect are tested with respect to the most variate principal components. Graphs of both stages show IVC and Batch have the highest and lowest significant effects on PCs, respectively. (C-D) Results displaying the major principal components of gene expression values based on IVCs. Percentages represent variance captured by the most variated principal components with the lowest batch effect for either stage. Day 6 (PC5) and day 14 (PC1) show the variation in the dataset with IVC as the main variable.

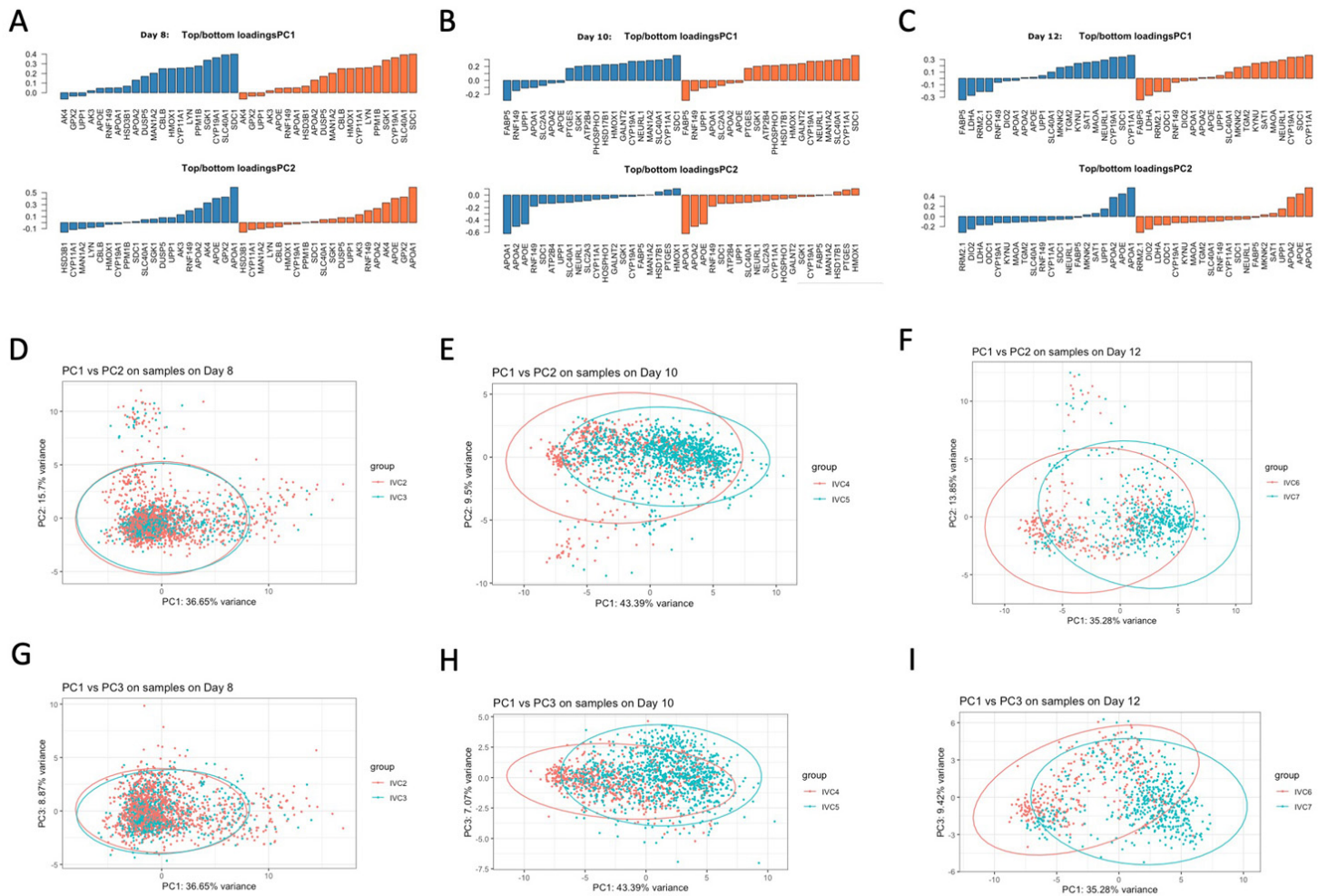


Fig.A 2: **PCA analysis A-C.** The top 20 genes with the most extreme loadings on each principal component for days 8, 10, and 12 are shown. Source of variance between samples for the top 20 genes in each stage. D-F. Results for major principal components of gene expression values based on IVCs for three stages (day 8, day 10, and day 12). Percentages represent variance captured by principal components on IVCs by controlling for batch effect.

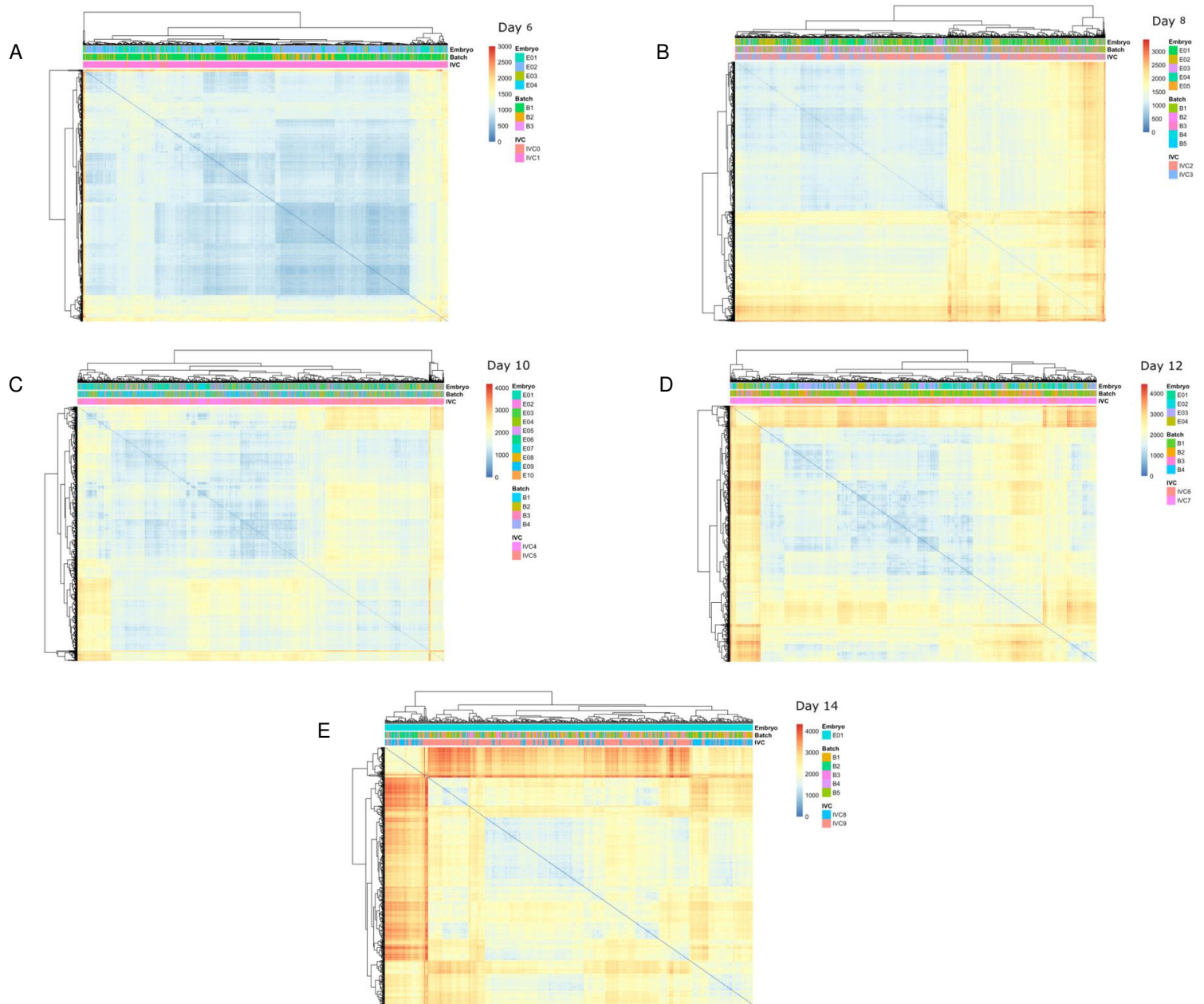


Fig.A 4: **Heatmap of Manhattan distance between samples in each stage.** Heatmaps show the samples at each stage that are closer in a cluster based on distance. The covariates are shown for days 6, 8, 10, 12, excluding day 14. Day 6 shows the majority of samples that have the smallest distance (only a few samples have the maximum distance). Samples collected for each day are clustered into two main groups indicating that the samples collected for day 6 have the greatest alignment, whereas day 14 samples are the least aligned.

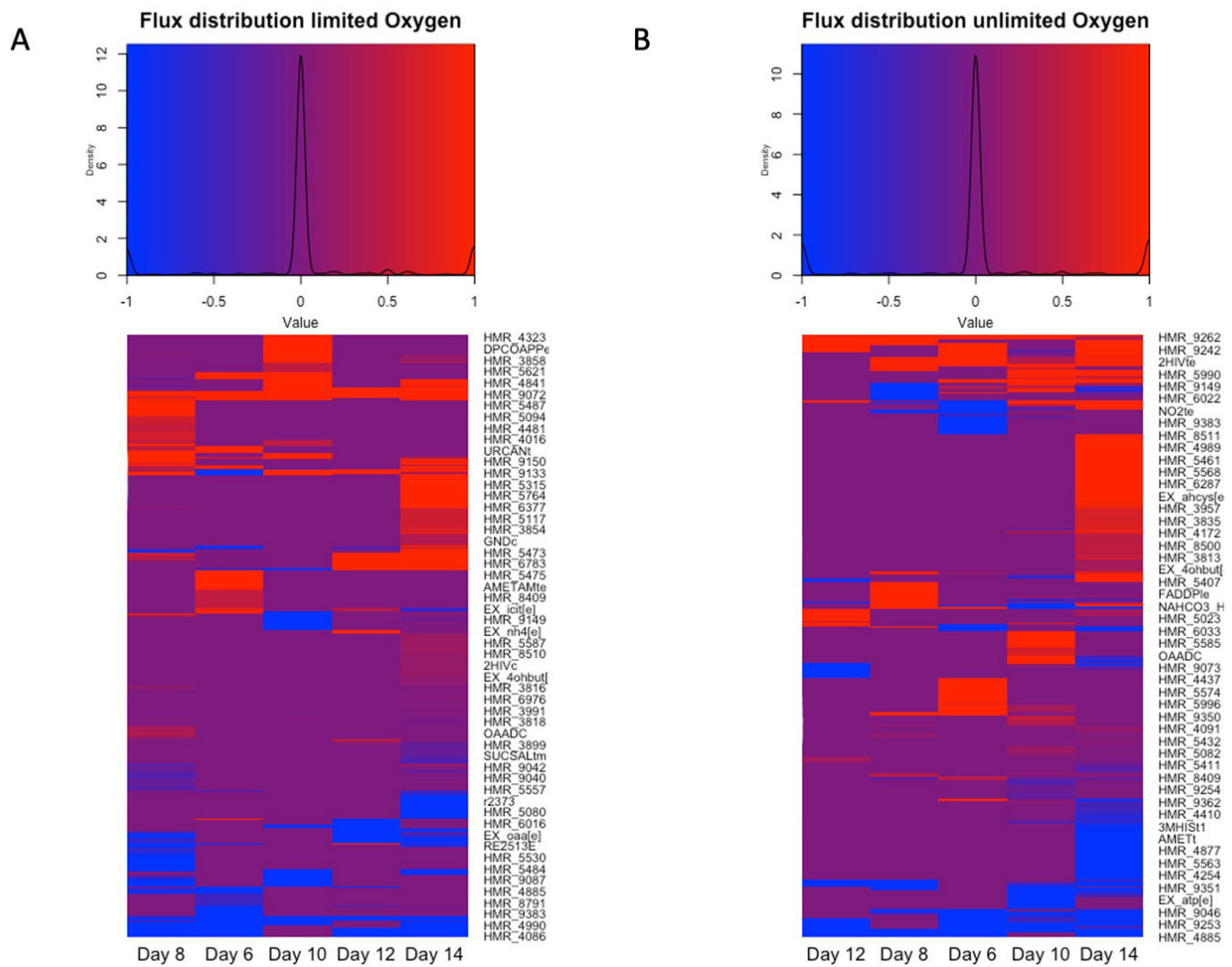


Fig.A 5: Heat map of flux distribution. (A) Oxygen uptake set to $-5 \text{ (mmol g}^{-1} \text{ h}^{-1})$. (B) Unlimited oxygen. Flux distribution of reactions across stages. Colors from blue to red represent non-zero reaction flux from low to high, respectively. Reaction IDs represent metabolic reactions provided by the human 1 dataset. There is a significant effect on flux rate by stage (ANOVA: $\alpha = 0.01$, P-Value = 0.007286) adjusting for the oxygen uptake.

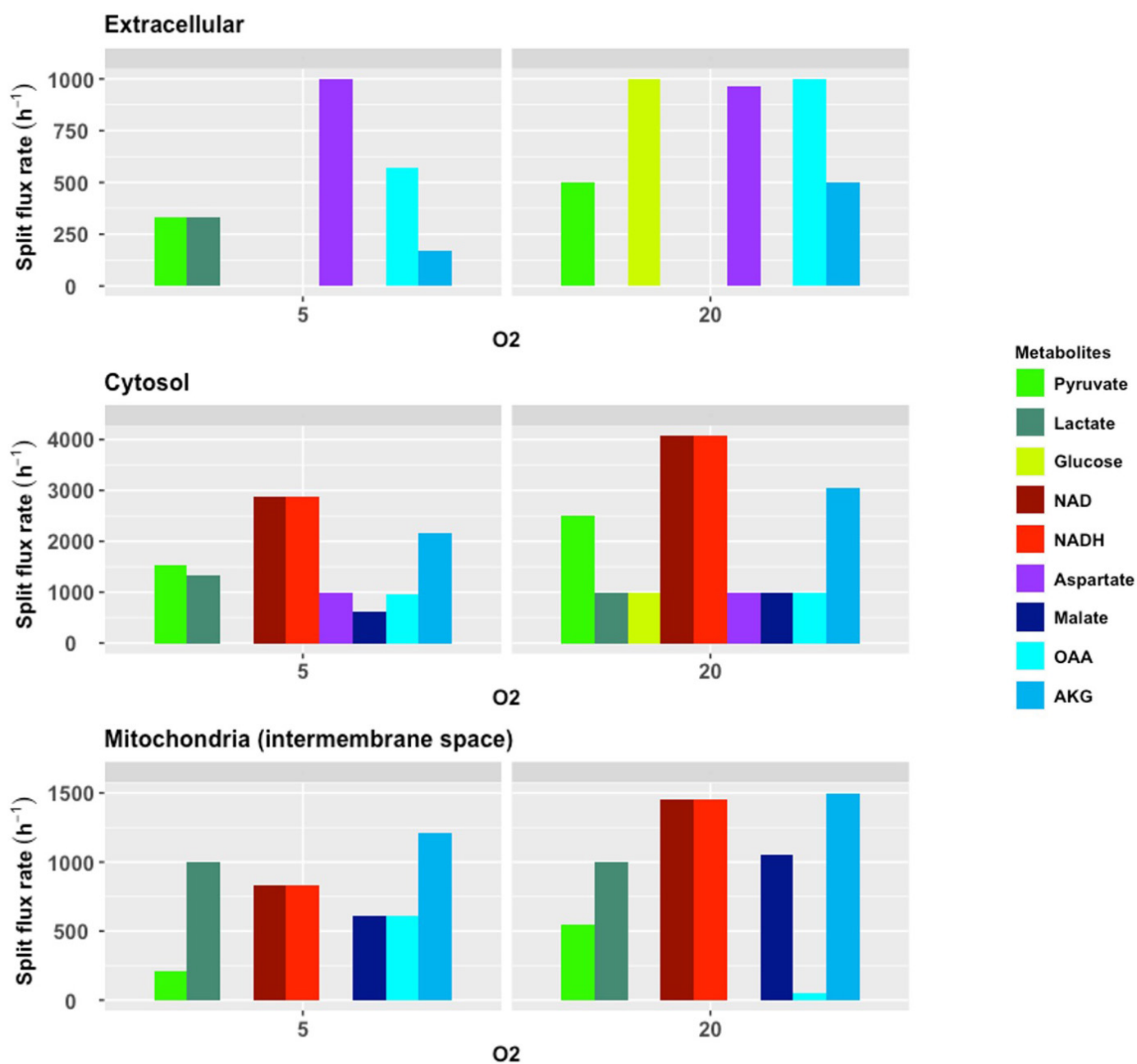


Fig.A 6: Bar graph of split flux in three compartments. Split flux for Day 14 MAS metabolites per compartment. 1. Extracellular, 2. Cytosol, and 3. Mitochondria. NAD⁺/NADH is constant for Mitochondria and Cytosol. Split flux indicates lactate transport into the mitochondrial intermembrane space.

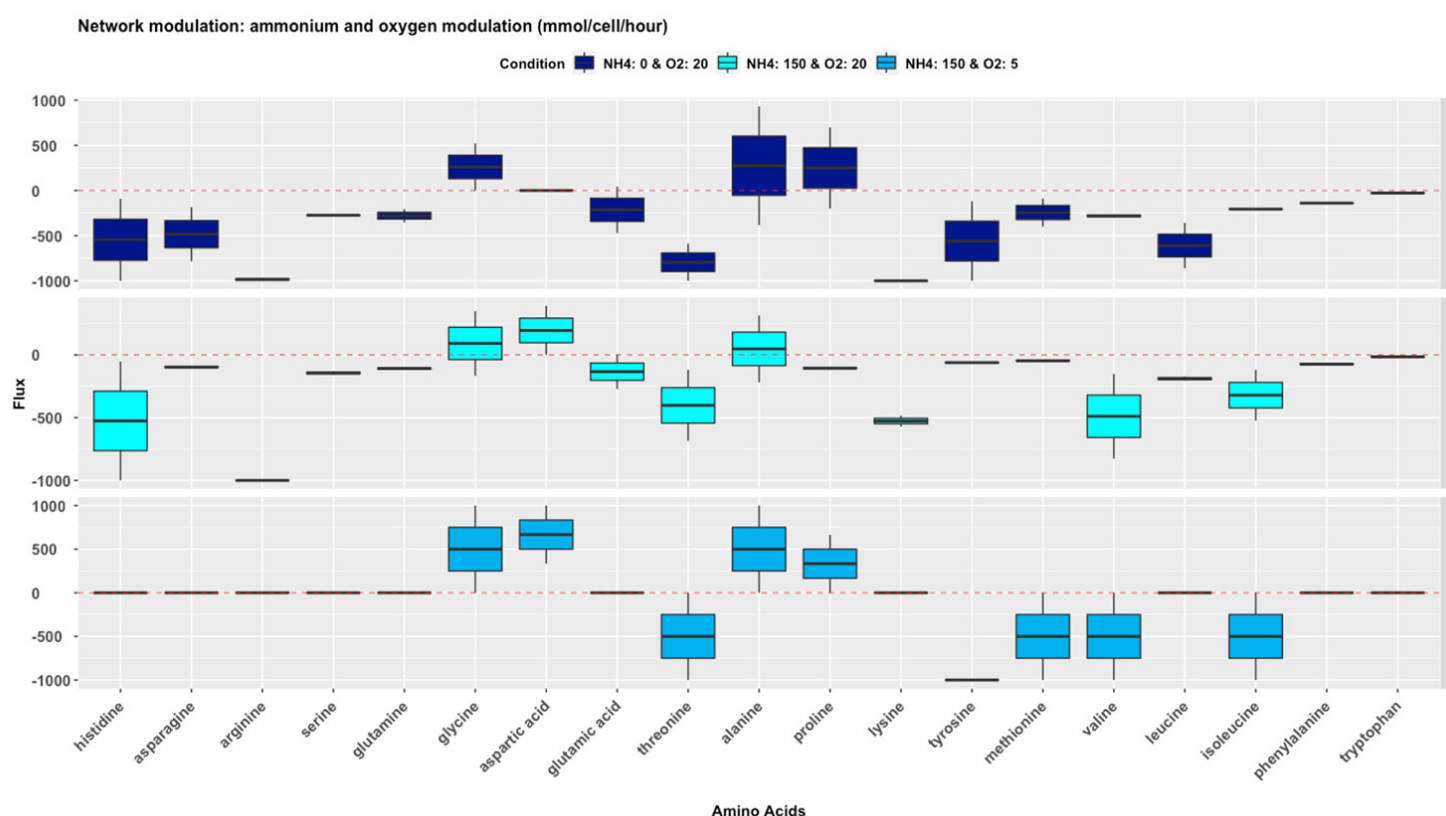


Fig.A 7: **Network modulation for 19 Amino acids in three conditions.** Reaction flux rate is shown for two stages that contain 19 amino acids. The average flux among the amino acids is significant ($P\text{-Value} \leq 0.05$) which indicates the mean difference flux among amino acids. The average flux of reactions is also influenced by adjusting oxygen and NH₄, but the effect is significant only when oxygen uptake is set to 5 and NH₄ is set to 150.

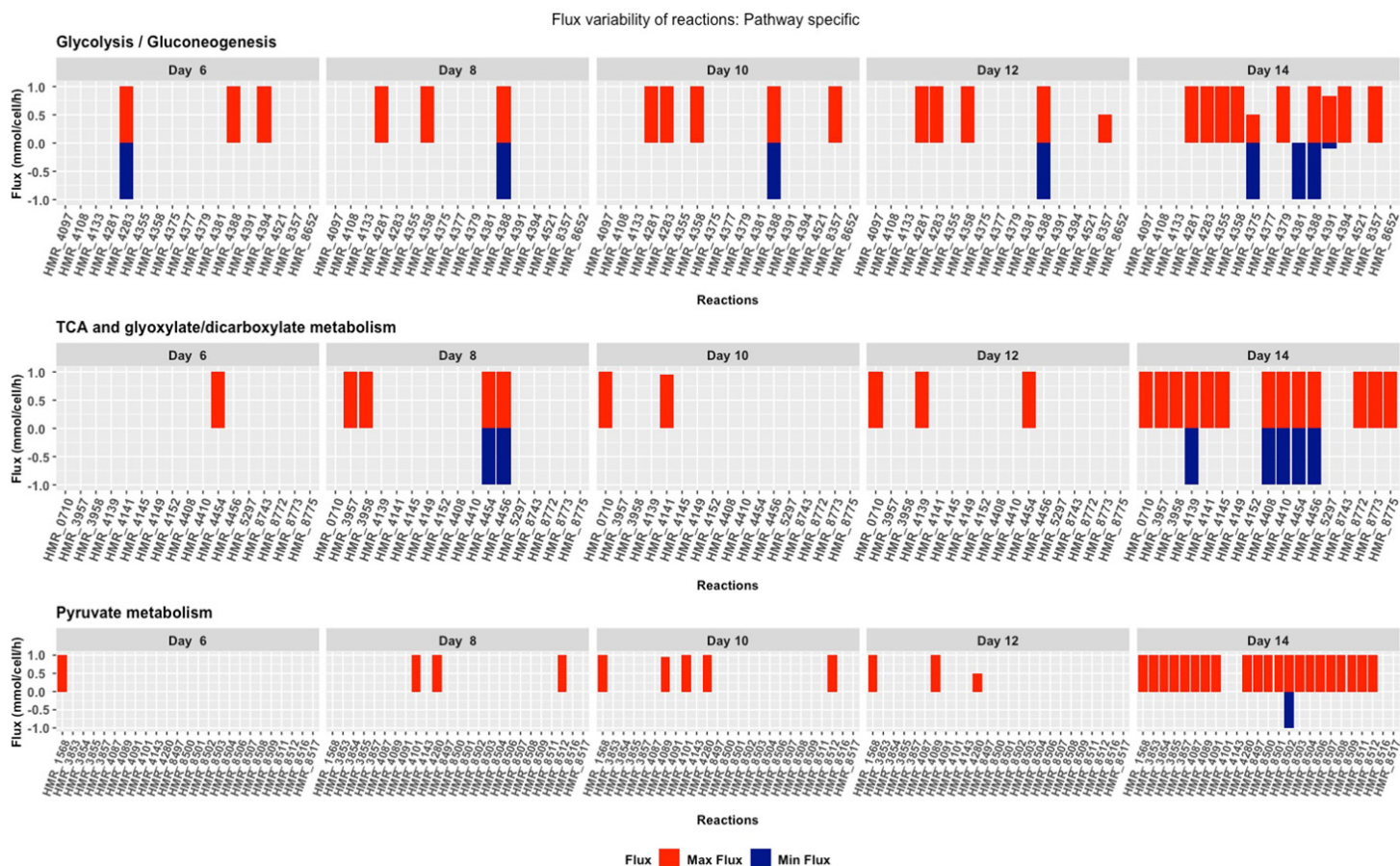


Fig.A 8: **Flux variability analysis of pathway specific reactions.** For each stage, the minimal and maximal flux of reactions per unit biomass is shown for three pathways: Glycolysis/Gluconeogenesis, TCA, and Pyruvate metabolism. The final stage is characterized by the greatest flux in variability. The X-axis represents the reaction ID from the Human 1 dataset. The Y-axis shows the flux rate per 1000 unit biomass.